Femoral Fracture Type can be Predicted from Femoral Structure:

A Finite Element Study validated by Digital Volume Correlation Experiments.

M. Ikhwan Z. Ridzwan[1, 2], Chamaiporn Sukjamsri[1,3], Bidyut Pal[1,4], Richard J. van Arkel[1], Andrew Bell[5], Monica Khanna[6], Aroon Baskaradas[7], Richard Abel[8], Oliver Boughton[8], Justin Cobb[8], and Ulrich N. Hansen[1]

[1]Department of Mechanical Engineering, Imperial College London, London SW7 2AZ, UK

[2]School of Mechanical Engineering, Engineering Campus, Universiti Sains Malaysia, 14300 Penang, Malaysia

[3]Department of Biomedical Engineering, Faculty of Engineering, Srinakharinwirot University, Nakhonnayok, 26120, Thailand

[4]School of Engineering, University of Portsmouth, Portsmouth, PO1 3DJ, UK

[5]MSC Software Ltd., 4 Archipelago, Lyon Way, Frimley, Surrey GU16 7ER, UK

[6]Department of Clinical Imaging, Imperial College Healthcare NHS Trust, London, UK

[7]Trauma and Orthopaedic Surgery, Imperial College Healthcare NHS Trust, London, UK

[8]Department of Surgery and Cancer, Imperial College London, Charing Cross Hospital, London W6 8RF, UK

ABSTRACT

Proximal femoral fractures can be categorised into two main types: neck and intertrochanteric fractures accounting for 53% and 43% of all proximal femoral fractures, respectively. The possibility to predict the type of fracture a specific patient is predisposed to would allow drug and exercise therapies, hip protector design and prophylactic surgery to be better targeted for this patient rendering fracture preventing strategies more effective. This study hypothesized that the type of fracture is closely related to the patient-specific femoral structure and predictable by finite element (FE) methods. Fourteen femora were DXA scanned, CT scanned and mechanically tested to fracture. FE-predicted fracture patterns were compared to experimentally observed fracture patterns. Measurements of strain patterns to explain neck and intertrochanteric fracture patterns were performed using a digital volume correlation (DVC) technique and compared to FE-predicted strains and experimentally observed fracture patterns. Although loaded identically, the femora exhibited different fracture types (6 neck and 8 intertrochanteric fractures). CT-based FE models matched the experimental observations well (86%) demonstrating that the fracture type can be predicted. DVC-measured and FE-predicted strains showed obvious consistency. Neither DXA-based BMD nor any morphologic characteristics such as neck diameter, femoral neck length or neck shaft angle were associated with fracture type. In conclusion, patient-specific femoral structure correlates with fracture type and FE analyses were able to predict these fracture types. Also, the demonstration of FE and DVC as metrics of the strains in bones may be of substantial clinical value, informing treatment strategies and device selection and design.

Keywords: neck; intertrochanteric; fracture; finite element analysis; digital volume correlation

INTRODUCTION

Proximal femoral fractures (PFF) can be categorised into two main types: femoral neck (intracapsular) and intertrochanteric (extracapsular) fractures accounting for 53% and 43%, respectively, of all PFF [1]. Each fracture type is treated with a specific type of operative treatment and has different potential complications to patients [2]. The ability to assess which fracture type a specific patient is predisposed to could aid fracture prevention strategies. It has been shown that by selecting specific exercise regimes [3; 4] or drug treatments [5] specific parts of the femoral structure can be targeted and strengthened, potentially reducing the risk of this fracture type. Hip protectors could be designed to preferentially protect against the type of fracture the specific patient is prone to. More controversially, knowledge of the likely fracture type could aid prophylactic surgery.

Several studies have been performed to identify the factors that determine the fracture type [6-16]. A summary of these studies suggests that intertrochanteric fractures were associated with femora with lower bone mineral density (BMD) and thinner cortices while femoral neck fractures were associated with structural features such as a higher neck shaft angle (NSA) and a longer femoral neck length (FNL). However, these findings were not consistent, often reporting no significant effects, and some of the results were contradictory. Most of these studies were clinical studies involving patients who had suffered a fracture. The results of such studies are difficult to interpret in terms of the structural features of the femur associated with the fracture type as other factors, such as fall direction [17], will also have an effect on the resulting fracture type.

To determine if the femoral structure alone predisposes a patient to a particular type of fracture this study aimed to isolate femoral structural features from other characteristics that may affect the

fracture type. To this end, cadaveric femora were tested under identical laboratory conditions, simulating a fall to investigate if these femora would exhibit different fracture types.

Any fracture has a degree of randomness resulting in a distribution of strength values. Thus the fracture type, may also have a seemingly random nature, the source of which may not be discernible from the overall structure assessed visually or from a CT scan. Hence, a CT based finite element (FE) analysis of each of the specimens was also carried out. The FE method is a frequently used tool for investigating femoral fracture load [12; 17-22] and its particular advantage in the context of our study is that it is entirely deterministic, containing no random elements. Thus, if the FE analysis predicts the experimental fracture types, then the fracture type is not determined by random effects but from features contained within the CT scan.

The hypothesis of this paper is that the femoral structure, including bone density distribution, as discernible from a CT-scan, determines if a patient is more predisposed to a femoral neck than to an intertrochanteric fracture. As part of the investigation it was assessed if the FE methodology could predict these fracture types. Thus, we assessed if FE may be used as a clinical tool for predicting the fracture type and aid in treatment planning. Finally, it was investigated if femoral characteristics, such as local BMD or femoral neck axis length, were associated with the fracture type.

MATERIAL AND METHODS

Femur Specimens and Preparation

Fourteen human cadaveric femora from eleven donors were obtained from Platinum Medical, Biological Resource Center, Phoenix, USA. The donors (mean age, 66.5±14.5 years; range: 42-86 years) were four males, specimens M1 to M4, and seven females, specimens F1 to F10. This study was approved by the National Research Ethics Service (NRES) Committee London – London Bridge, United Kingdom (Ethics reference number: 12/LO/0797). The soft tissues were removed from the femora, and all femora were cut approximately 15 cm from the distal articular surface. The specimens were stored at -20°C and thawed to room temperature for specimen preparation as well as prior to dual energy X-ray absorptiometry (DXA), CT scanning and mechanical testing.

Imaging Methods

The femora were radiographed, CT and DXA scanned. CT images were used for generating 3D FE models. Radiographs were used for measuring femoral geometrical characteristics while the DXA measurements were used to quantify BMD. Femora were scanned with a Philips, 64 slice CT scanner. The slice thickness was 1 mm. The settings were 120kV, 70mAs, and a 512 x 512 pixels image matrix with pixel size between 0.8 to 1.0 mm. In-vitro DXA scans of the cadaveric femora, submerged in a water bath and positioned to replicate the routine clinical practice of supine patient position with the femur in 20-25° of internal rotation, were performed using GE Lunar Prodigy.

In-Vitro Mechanical Testing

The mechanical testing to fracture of the 14 femora was divided into two parts, twelve of the femora were tested in Part 1, while the remaining 2 femora, F7 and F10, were tested in Part 2. The mechanical set-up in Part 1 and Part 2 was conceptually the same (Figure 1), only the set-up in Part 2 was modified to be placed within a CT scanner, enabling CT scanning of the loaded specimen. In Part 1 the purpose was simply to record the fracture type and fracture load. In Part 2, in addition to recording to the fracture type and load, the specimen was CT-scanned at incrementally increasing loads until final failure. These CT scans were analysed using Digital Volume Correlation analysis (DVC) which measures the increasing strains within the femur during loading by tracking the grey scale patterns within the CT images as these patterns are deformed during loading. The main purpose of Part 2 was to provide strain fields close to fracture which could be used to further validate the FE fracture simulation.

Part 1: In-Vitro Mechanical Testing within an Instron Test Machine

To represent a sideways fall configuration each femoral shaft was positioned 10° from horizontal and the femoral neck axis internally rotated by 15° relative to a vertical axis (Figure 1) [23-25]. The femur was fixed at the distal end allowing the distal end to rotate freely around the axis normal to the plane of Figure 1. The medial aspect of the femoral head and the lateral aspect of the greater trochanter were covered with PMMA to prevent local crushing and simulating the effect of soft tissue cover [24]. Each femur was loaded to failure defined as the peak of the load-deformation curve using an Instron 8874 testing machine (Instron Corporation, Canton, MA). A constant vertical displacement of 6.6 mm/s was applied to the femoral head which rested on an x-y table to eliminate

any reaction forces. Load and displacement data were sampled at 1000 Hz. The load was measured using a uniaxial load cell. This load cell had a full-range of ±10 kN and was accurate to 0.5% of the indicated load.

Part 2: In-Vitro Mechanical Testing within a Clinical CT Scanner and DVC Strain Analysis

In part 2 a CT-compatible custom-designed loading device was used. The set-up was conceptually the same as in Part 1 but the load was introduced by turning a Hex screw and measuring the load using a compression load cell (LBM-1000, Interface Force Measurements Ltd.) (Figure 1). The device was designed and positioned within the CT scanner in such a way that there were no metal components in the field of the CT scan thereby avoiding metal artefacts in the images. Patient scan settings of 120 kVp and 60 mAs were used. The compressive load was applied to the femoral head in increments of approximately 500 N. At the end of each increment a CT scan was performed. To reduce stress relaxation effects during the 4.4 seconds of the CT scan the specimen was held for 5 minutes prior to scanning which allowed the load to stabilise and no change in load could be detected during the scan. This process of incremental loading and CT imaging was continued until final failure.

DVC uses digital image tracking to determine the displacement of patterns of voxel grey scale values in two sequential CT images of bone under increasing load. As the method utilises CT scans, the DVC method has the ability, uniquely amongst experimental methods, to assess the internal strains in bone [26-28]. Previous studies were based on micro-CT imaging and a novel aspect of this study was the use of DVC based on clinical CT images. The CT image files were imported

into commercial DVC software (DaVis 8.1.6, LaVision, Goettingen, Germany). Two scans were taken at zero load and confirmed that the maximum noise levels were 0.0003 and -0.0005 for the maximum and minimum strains, respectively, which had a negligible effect on the measured strain values. Software settings were: subvolume size sequences of 96x96x96, 76x76x76, and 48x48x48 voxels/mm, 75% overlap and a correlation degree of 0.94. The software calculated the distribution of principal strains throughout the loaded femur. The DVC-measured strain distributions were compared with the FE-predicted strain patterns and the fracture patterns observed during mechanical testing.

FE Model of Proximal Femur

The CT dataset of the cadavers were segmented using medical image analysis software (Avizo, Version 6.3, Visualization Sciences Group, Burlington, MA, USA). The datasets had an average of 280 CT slices that covered the proximal head to about 25 cm down the shaft of the femur from the greater trochanter. Surface models were generated and exported to the FE software (Marc/Mentat 2013, MSC Software Corp., Santa Ana, CA, USA) to develop three-dimensional FE models of the femur. The models were meshed using linear 4-node tetrahedral solid elements. Mesh convergence analyses of three key results were performed: the load to initiation of failure (prior to deactivation of elements); the ultimate fracture load and the predicted fracture type. The converged meshes contained approximately 70,000 nodes and had an average element edge length of 1.3 mm (Figure 2).

Bone was modelled as a linear and isotropic material. The elastic modulus of each bone element was determined from the Houndsfield Units (HU) of the CT image using a previously established

procedure [29]. Specifically, the bone apparent density (ρ_{app} in g/cm^3) was calculated using a linear relationship $\rho_{app} = 0.00089\ HU + 0.035$ and the Young's Modulus from $E = 6.850\ \rho_{app}^{1.49}$. A Poisson's ratio of 0.3 was assumed.

The FE closely simulated the experimental set-up in Figure 1. The distal end was fixed apart from rotation around the axis normal to the plane of Figure 1. Nodes corresponding to the area covered by PMMA in the experiments (the trochanteric area) were constrained in the vertical direction. The vertical load applied to the surface of the femoral head was distributed on nodes over an area of approximately 3 cm in diameter. Femoral failure was predicted using maximum/minimum principal strain criteria. The maximum and minimum principal strains to failure used for both cortical and cancellous bone were 0.62% and -1.04%, respectively [30; 31].

Assessing the FE-predicted fracture type based on just one element or a small area that first reaches the critical failure threshold was not considered sufficiently accurate since an initial failure may get arrested with subsequent failure initiating in another region of the femur. For these reasons a progressive FE failure simulation was adopted. Elements that met the principal strain failure criterion mentioned earlier were considered failed and automatically deactivated from the analysis during the iterative solution procedure (Figure 2). The use of iterative-level, load stepping constraints in Marc ensured convergence during the deactivation. A Newton-Raphson iterative scheme was used which meant that the onset of complete failure was numerically indicated by a reduced load in a subsequent increment.

Definition of Fracture Types

In both the physical experiment and in the FE models the specimens were tested until peak load which coincided with major but not complete fracture of the bone and as a result fractures were never displaced. A fracture that was contained within the intracapsular region (including subcapital and any variation of a fracture of the cervical neck) was defined as a neck fracture whilst a fracture that was contained within the extracapsular region (including fractures that were limited to or involved the greater trochanter, lesser trochanter, intertrochanteric region and subtrochanteric fractures) was defined as an intertrochanteric fracture. Fractures at the interface of the two regions (involving the basicervical region and extending outside the capsule into the intertrochanteric region running parallel to the basicervical region) were also categorised as intertrochanteric fractures due to these fractures being treated as extracapsular fractures in the clinical setting [32]. The classification of fractures was carried out blinded by three independent observers (MIZR, OB, & UNH); in cases of disagreement, the fracture type was classified according to the majority.

Femoral Characteristics

From DXA scans and 2D anterior-posterior radiographs (Figure 3) of the 14 specimens the total BMD, neck BMD, Ward's triangle BMD, greater trochanteric BMD, isthmus cortical index (CI), neck diameter (ND), femoral neck length (FNL) and neck shaft angle (NSA) were measured to determine which, if any, parameters were associated with fracture type.

Statistical Analysis

Inter-rater reliability was assessed using Fleiss' kappa [33]. All other data were analysed in SPSS (version 22, SPSS Inc., Chicago, Illinois) with the significance level set at $p < 0.05$. First, the correlation between the measured experimental fracture load and both BMD and FE-predicted fracture load was assessed with Pearson's product-moment correlation. Then the data were split into the two fracture groups, neck fracture or intertrochanteric and a Fisher's Exact Test was used to assess the association between the FE-predicted fracture types and the observed experimental fractures types. Finally, differences between specimen characteristics of the two fracture groups were analysed with unpaired t-tests.

RESULTS

The experimental and FE-predicted fracture loads and types are listed in Table 1 which also shows the total BMD values for each sample. Fracture load for specimen M4 was not recorded due to a technical error when collecting data and was not included for correlation statistics. Specimen M1 was identified as a potential outlier as it had a BMD 1.5 times the interquartile range greater than the upper quartile of other specimens. A patient with such dense bone is unlikely to fracture and hence correlation data is presented both with and without this specimen. As expected, there was a strong correlation between increasing BMD and increasing experimental fracture load ($r = 0.82$ with M1, $r = 0.63$ without M1, $p < 0.029$ both with and without M1; Figure 4). There was an even stronger correlation between increasing FE-predicted fracture load and increasing experimental fracture load ($r = 0.90$ with M1, $r = 0.75$ without M1, $p < 0.005$ both with and without M1, Figure 4). The FE model predicted the experimentally observed fracture type 86 % of the time (Table 2, 95 % CI: *65-100 %*, Fisher's Exact $p = 0.026$). The inter-rater reliability (Fleiss' kappa) for assessing these fracture types was 0.95.

The fracture types that occurred in the experimental rig were consistent with the FE-predicted and DVC-measured strain patterns (Figure 5). The two specimens that were used for this DVC analysis had notably different bone quality. F7 was osteopenic (T-score: -2.1) and F10 was osteoporotic (T-score: -4.3) and the two specimens exhibited different fracture types. The DVC strain measurements show the strain just prior to fracture and, consistent with the FE predictions and experimental fracture type, high strain concentrations can be noted in the neck and trochanteric regions, respectively. The FE and DVC assessments of strain were remarkably similar in regards to qualitative patterns as well as quantitative values. Thus, DVC strain measurements corroborated the FE predictions, both seemingly able to explain the fracture type.

No anatomic element was able to distinguish between fracture types in this small study (Table 3). No differences in any BMD measurements at any locations were detected between the fracture groups; neither for the entire group (all $p \geq 0.08$), or for female only specimens (all $p \geq 0.07$). However, there was a trend that specimens that fractured in the intertrochanteric region failed at lower loads, and had lower BMD than those that fractured at the neck. No other difference between the two fracture-groups were detected for any of the other variables: gender, age, height, weight, BMI, Isthmus CI, neck diameter, FNL and NSA; neither for the entire group (all $p \geq 0.21$), nor for female-only specimens (all $p \geq 0.21$).

DISCUSSION

This study investigated whether the femoral fracture type was random or if it could be predicted from the femoral structure based on a CT scan. Femora loaded in an identical manner resulted in a mix of fractures (6 neck fractures and 8 intertrochanteric fractures) reflecting clinical reality [1], and giving credibility to the experimental set up. DXA-scores correlated well with the energy required to cause a fracture confirming the relevance of this imaging modality in the assessment of fracture risk. However, DXA was unable to distinguish between the types of fracture – no statistically significant differences were found between the fracture groups and BMD. In contrast, the FE model accurately predicted both the fracture load and the fracture pattern.

Keyak, et al. [12] and Pulkkinen, et al. [9] also reported a mix of fracture types when testing cadaver femora loaded in an identical manner (10 neck versus 4 intertrochanteric and 88 neck versus 51 intertrochanteric fractures, respectively). Keyak, et al. [12] and Koivumaki, et al. [8] compared FE-predicted fracture types to in-vitro cadaver fracture types and found degrees of matching of 79% and 85%, respectively, supporting the predictive capability of FE found in our study.

In contrast to the FE modelling approaches by Keyak, et al. [12] and Koivumaki, et al. [8] our study modelled the progression of fracture from initiation to final failure. Keyak et al. predicted only the initial failure of a small area. If this area coincided with any part of the much larger experimentally observed fracture region it was considered a match. Such a strategy is likely to over-predict the degree of matching. Koivumaki et al. did not predict fracture but related the strain in the greater trochanteric region to the strain in the neck region. The region with the larger strain was predicted

to fracture. While our approach of simulating the progressing fracture and comparing like with like (fracture type with fracture type) did not vastly improve the degree of matching over those earlier studies it may arguably be more reliable.

The FE models statistically explained 57% of the variability seen in experimental fracture loads whereas DXA BMD-measurements were only able to explain 39% of the variability (Figure 4). These findings are consistent with Cody, et al. [34] and Orwoll, et al. [35] who also found FE to be superior in this aspect and to the findings of Cheng, et al. [36] who reported an R^2 value of 0.76 between total BMD and femoral strength. Cheng et al. also report femoral strengths (3.98kN ± 1.6kN) which are comparable to the results of our study.

Mautalen, et al. [15], in a comprehensive review of clinical studies, reports low BMD to be associated with intertrochanteric fractures. However, Dretakis, et al. [37] and Maeda, et al. [7] did not find a significant effect and Pulkkinen, et al. [9] reports lower strength (closely related to low BMD) to be associated with neck fractures. In our study, the intertrochanteric group had a nominally lower BMD (Table 3) which would be consistent with most previous studies, however, this result was not statistically significant. Our finding may be a type II statistical error due to the low power of the study as discussed below. The fact that the FE methodology, which includes any effect of low BMD, and despite the low power of the study exhibited a strong ability to predict the fracture types indicates the strength of this method over DXA.

Cheng, et al. [36] reported neck, Ward's triangle and greater trochanteric BMD values in females of 0.676 g/cm^2, 0.515 g/cm^2 and 0.612 g/cm^2, respectively, which compares reasonably with the values found in our study (Table 3). Previous studies have reported an association between the location of BMD and the fracture type; low neck BMD being associated with neck fractures [6] and low trochlear BMD being associated with intertrochanteric fractures [11; 15], while Maeda, et al. [7] did not find a significant association. In our study we also did not find such an association. Maeda, et al. [7] did find that a low Isthmus CI, suggested to reflect a general thinning of the cortices including the neck and trochanteric regions, was associated with intertrochanteric fractures. In our study we did not find such an association. However, the cortices at the isthmus were approximately 8 mm thick and considering the CT scan voxel dimension of ~ 1 mm it may be that the inaccuracy of our measurements prevented us from finding an association.

Pulkkinen, et al. [9] reported ND, FNL and NSA values for females with neck fractures of 3.06 cm, 9.7 cm and 126°, respectively, which compares well with the values found here (Table 3). A wide and short femoral neck, and a low neck shaft angle all theoretically strengthen the femur against a femoral neck fracture and predispose the femur towards an intertrochanteric fracture. Such associations have been reported previously [7; 11; 14] although in other studies such associations were not found Dretakis, et al. [37]. In our study we did not find an association between these parameters and fracture type.

An important limitation affecting all the above findings was the limited number of samples. Notably, any differences in fracture strength and BMD values failed to differentiate statistically between the fracture groups. However, the p-values for these analyses were not far from the

statistical significance threshold of 0.05 (Table 3). Another limitation of the study was the subjective judgment made when classifying fractures into neck or intertrochanteric fracture. However, the three observers assessed the fracture types with inter-rater reliability of 0.95, suggesting that the reliability of the classification was not a severe limitation.

We used a loading rate of 6.6 mm/s comparable to that used in similar studies[18; 38; 39] but much lower than the loading rate during a sideways fall of ~100 mm/s[23]. Courtney et al. (1994)[23] found that fracture load increased but energy to fracture was unaffected by loading rate. As the energy to fracture was unaffected it seems likely that also the fracture type would be unaffected by loading rate. Based on Courtney's work, we expect that our study underestimated the fracture load by about 20% but did not change the fracture type.

There are several limitations of the FE modelling that may explain why 14% of fracture types were not predicted accurately. The FE model did not include features that are not captured by the CT image such as the presence of microcracks, differences in bone mineral crystallinity, or changes in bone collagen with age. The effect of such factors on the resulting fracture type will appear random in the context of the FE model used in this research. Another notable uncertainty involves details to reflect the real conditions of the impact to the greater trochanter during a fall (a complexity shared with the experimental set-up). However, too rigid or blunt a support would lead to high rates of trochanteric fractures which we did not find and may indicate that the effect of this limitation is minor. Finally, the fracture of bone is likely to be affected by the anisotropic mechanical properties of bone, including strength, which was not simulated.

Although initially introduced as a validation tool for the FE-predicted strains, the DVC component is an important additional outcome of the study. The DVC measured the strains throughout the bone and showed areas of critical strains indicating the location of imminent failure and showed remarkable agreement with the FE predictions in regards to both strain patterns and quantitative strain values. Interestingly, the DVC and FE assessments of F7 show that the strains in the regions of high tensile strain at the inferior aspect of the neck and high compressive strain at the superior aspect of the neck are both near the critical strain values of 0.62% and -1.04% for tension and compression, respectively. Hence, the femoral neck fracture may involve a complicated mix of tensile and compressive fracture.

Internal strains in bone have previously been measured using DVC [28] based on micro-CT images. However, in our study the analysis was based on images from a clinical CT-scanner. Prior to this study it was not clear that such an analysis would be possible. The feasibility of using clinical CT scans opens up the possibility of measuring internal bone strains also in patients and enables a great range of possible applications.

This study demonstrated that from an FE assessment of a patient's femoral structure it is possible to evaluate if the patient is prone to suffer a neck or an intertrochanteric fracture, thus, a hip protector, exercises or drug therapy that protects against the specific fracture type can be chosen. Also the study developed a novel DVC technique based on clinical CT scans which may have substantial clinical significance. The technique may be applied to measure the strains around

implants in patients, thereby monitoring the status of the fixation as part of patient follow-up or aid in the development of implants resulting in more benign stresses around the implant. Another major use of the DVC technique may be the assessment of the bone strains in patients under abnormal loading caused by, for example arthritis or bone deformities, providing unique information for the understanding and subsequent treatment of these pathologies.

AUTHOR'S CONTRIBUTIONS

Research design: MIZR, BP, JC, and UNH. Data analysis and interpretation: MIZR, CS, BP, RJvA, ABell, MK, AB, RB, OB, JC, and UNH. Drafting of manuscript: MIZR, BP, RJvA, OB, and UNH. Revision of manuscript: CS, ABell, MK, AB, RA, and JC. All authors have read and approved this manuscript.

ACKNOWLEDGMENTS

The authors would like to acknowledge assistance from Shirley Fetherston, Fiona Watson and Lesley Honeyfield of the Imperial College Healthcare NHS Trust for technical assistance. This work was sponsored by Malaysia-Imperial Doctoral Programme (MIDP).

REFERENCES

1. AIHW. 2010. The problem of osteoporotic hip fracture in Australia. Buletin no 76 CAT. no. AUS121. Canberra: AIHW.
2. Evans PJ, McGrory BJ. 2002. Fractures of the proximal femur. Hosp Physician 38:30-38.

3. Heinonen A, Mantynen J, Kannus P, et al. 2012. Effects of high-impact training and detraining on femoral neck structure in premenopausal women: a hip structural analysis of an 18-month randomized controlled exercise intervention with 3.5-year follow-up. Physiother Can 64:98-105.

4. Nikander R, Kannus P, Dastidar P, et al. 2009. Targeted exercises against hip fragility. Osteoporos Int 20:1321-1328.

5. Keaveny TM, Hoffmann PF, Singh M, et al. 2008. Femoral bone strength and its relation to cortical and trabecular changes after treatment with PTH, alendronate, and their combination as assessed by finite element analysis of quantitative CT scans. J Bone Miner Res 23:1974-1982.

6. Hong TH, Moon KH. 2015. Localized femoral BMD T-scores according to the fracture site of hip and the evaluation of the sensitivity of the high risk group designated by FRAX® in hip fracture patients. Osteoporosis and Sarcopenia 1:109-114.

7. Maeda Y, Sugano N, Saito M, et al. 2011. Comparison of femoral morphology and bone mineral density between femoral neck fractures and trochanteric fractures. Clin Orthop Relat Res 469:884-889.

8. Koivumaki JE, Thevenot J, Pulkkinen P, et al. 2010. Does femoral strain distribution coincide with the occurrence of cervical versus trochanteric hip fractures? An experimental finite element study. Med Biol Eng Comput 48:711-717.

9. Pulkkinen P, Eckstein F, Lochmuller EM, et al. 2006. Association of geometric factors and failure load level with the distribution of cervical vs. trochanteric hip fractures. J Bone Miner Res 21:895-901.

10. Gomez-Benito MJ, Garcia-Aznar JM, Doblare M. 2005. Finite element prediction of proximal femoral fracture patterns under different loads. J Biomech Eng 127:9-14.

11. Gnudi S, Ripamonti C, Lisi L, et al. 2002. Proximal femur geometry to detect and distinguish femoral neck fractures from trochanteric fractures in postmenopausal women. Osteoporos Int 13:69-73.

12. Keyak JH, Rossi SA, Jones KA, et al. 2001. Prediction of fracture location in the proximal femur using finite element models. Med Eng Phys 23:657-664.

13. Fox KM, Magaziner J, Hebel JR, et al. 1999. Intertrochanteric versus femoral neck hip fractures: differential characteristics, treatment, and sequelae. J Gerontol A Biol Sci Med Sci 54:M635-640.

14. Duboeuf F, Hans D, Schott AM, et al. 1997. Different morphometric and densitometric parameters predict cervical and trochanteric hip fracture: the EPIDOS Study. J Bone Miner Res 12:1895-1902.

15. Mautalen C, Vega E, Einhorn T. 1996. Are the etiologies of cervical and trochanteric hip fractures different? Bone 18:S133-S137.

16. Mautalen C, Vega E. 1993. Different characteristics of cervical and trochanteric hip fractures. Osteoporos Int 3:102-105.

17. Bessho M, Ohnishi I, Matsumoto T, et al. 2009. Prediction of proximal femur strength using a CT-based nonlinear finite element method: differences in predicted fracture load and site with changing load and boundary conditions. Bone 45:226-231.

18. Pottecher P, Engelke K, Duchemin L, et al. 2016. Prediction of hip Failure load: In Vitro Study of 80 Femurs Using Three Imaging Methods and Finite Element Models—The European Fracture Study (EFFECT). Radiology 280:837-847.

19. Wakao N, Harada A, Matsui Y, et al. 2009. The effect of impact direction on the fracture load of osteoporotic proximal femurs. Med Eng Phys 31:1134-1139.

20. Keyak JH, Rossi SA, Jones KA, et al. 1997. Prediction of femoral fracture load using automated finite element modeling. J Biomech 31:125-133.

21. Ford CM, Keaveny TM, Hayes WC. 1996. The effect of impact direction on the structural capacity of the proximal femur during falls. J Bone Miner Res 11:377-383.

22. Lotz J, Cheal E, Hayes W. 1995. Stress distributions within the proximal femur during gait and falls: implications for osteoporotic fracture. Osteoporos Int 5:252-261.

23. Courtney AC, Wachtel EF, Myers ER, et al. 1994. Effects of loading rate on strength of the proximal femur. Calcif Tissue Int 55:53-58.

24. de Bakker PM, Manske SL, Ebacher V, et al. 2009. During sideways falls proximal femur fractures initiate in the superolateral cortex: evidence from high-speed video of simulated fractures. J Biomech 42:1917-1925.

25. Dragomir-Daescu D, Op Den Buijs J, McEligot S, et al. 2011. Robust QCT/FEA models of proximal femur stiffness and fracture load during a sideways fall on the hip. Ann Biomed Eng 39:742-755.

26. Hussein AI, Mason ZD, Morgan EF. 2013. Presence of intervertebral discs alters observed stiffness and failure mechanisms in the vertebra. J Biomech 46:1683-1688.

27. Madi K, Tozzi G, Zhang QH, et al. 2013. Computation of full-field displacements in a scaffold implant using digital volume correlation and finite element analysis. Med Eng Phys 35:1298-1312.

28. Bay BK, Smith TS, Fyhrie DP, et al. 1999. Digital volume correlation: Three-dimensional strain mapping using X-ray tomography. Experimental Mechanics 39:217-226.

29. Tuncer M, Cobb JP, Hansen UN, et al. 2013. Validation of multiple subject-specific finite element models of unicompartmental knee replacement. Med Eng Phys 35:1457-1464.
30. Bayraktar HH, Morgan EF, Niebur GL, et al. 2004. Comparison of the elastic and yield properties of human femoral trabecular and cortical bone tissue. J Biomech 37:27-35.
31. Keyak JH, Rossi SA. 2000. Prediction of femoral fracture load using finite element models: an examination of stress- and strain-based failure theories. J Biomech 33:209-214.
32. Massoud EI. 2010. Fixation of basicervical and related fractures. Int Orthop 34:577-582.
33. Geertzen J. 2012. Inter-Rater Agreement with multiple raters and variables. Retrieved December 5, 2016, from https://nlp-mlio/jg/software/ira/.
34. Cody DD, Gross GJ, Hou FJ, et al. 1999. Femoral strength is better predicted by finite element models than QCT and DXA. J Biomech 32:1013-1020.
35. Orwoll ES, Marshall LM, Nielson CM, et al. 2009. Finite element analysis of the proximal femur and hip fracture risk in older men. J Bone Miner Res 24:475-483.
36. Cheng XG, Lowet G, Boonen S, et al. 1997. Assessment of the strength of proximal femur in vitro: relationship to femoral bone mineral density and femoral geometry. Bone 20:213-218.
37. Dretakis EK, Papakitsou E, Kontakis GM, et al. 1999. Bone mineral density, body mass index, and hip axis length in postmenopausal cretan women with cervical and trochanteric fractures. Calcif Tissue Int 64:257-258.
38. Pulkkinen P, Jamsa T, Lochmuller EM, et al. 2008. Experimental hip fracture load can be predicted from plain radiography by combined analysis of trabecular bone structure and bone geometry. Osteoporos Int 19:547-558.

39. Nishiyama KK, Gilchrist S, Guy P, et al. 2013. Proximal femur bone strength estimated by a computationally fast finite element analysis in a sideways fall configuration. J Biomech 46:1231-1236.

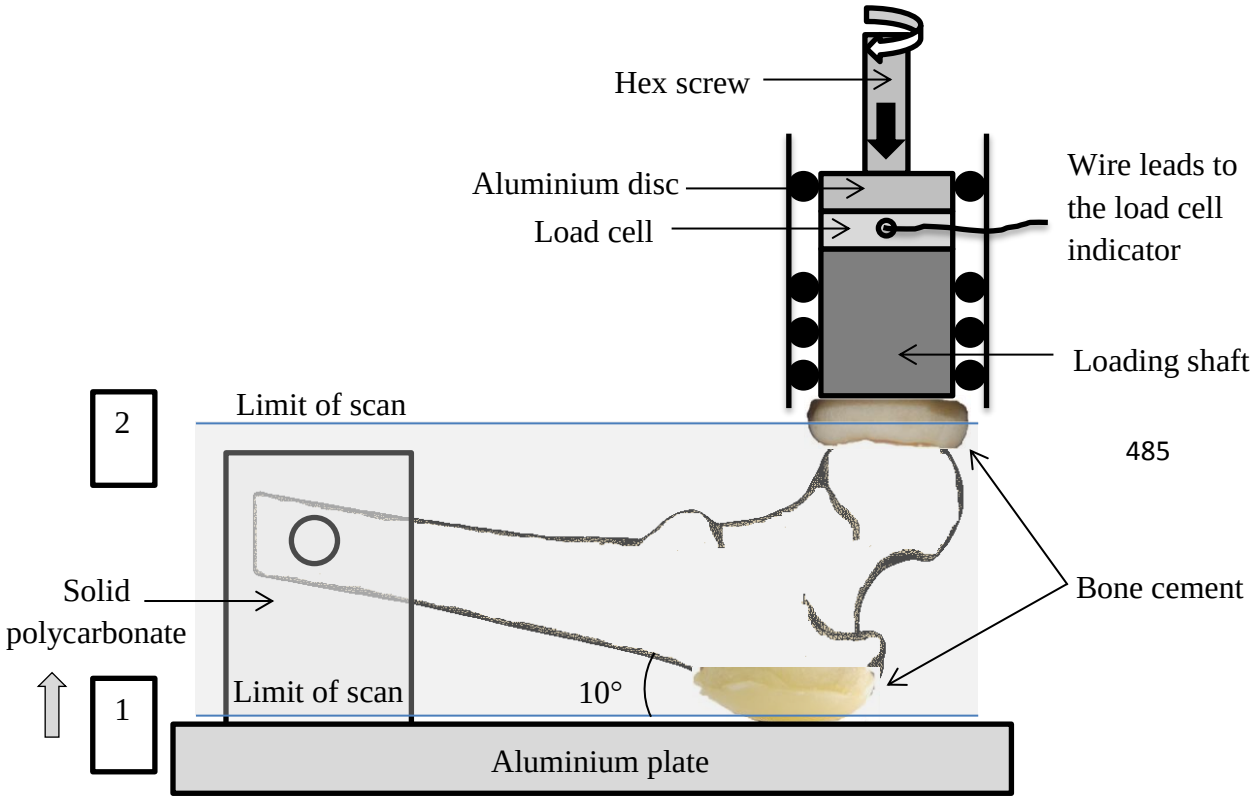

Figure 1 – Schematic diagram of the mechanical test-setup for Part 2 of the mechanical testing which is carried out within a CT scanner. The CT scanning started from position 1 moving to position 2. The resulting scan volume contained no metal components and no metal artifacts. For Part 1 of the mechanical testing the fixture above was placed within a standard Instron Mechanical testing machine and the load introduced via the cross head and load cell of the Instron (replacing the load device shown in the upper part of the figure). Also, for part 1 the bottom Aluminium plate was replaced by an x-y table.

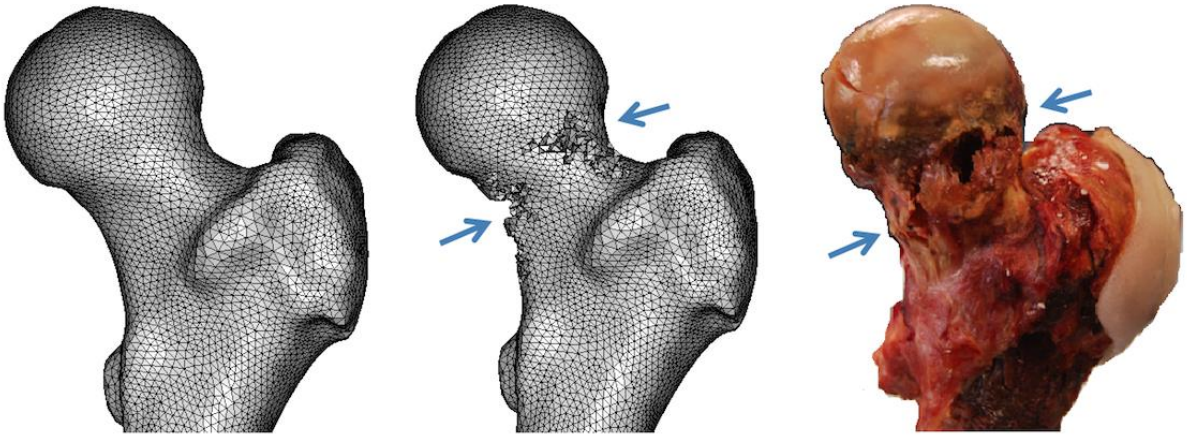

(a) (b) (c)

Figure 2 – (a) FE meshed model before initiation of fracture and (b) the same model with deleted elements at the point of ultimate fracture load and (c) the actual fractured femur that was simulated (specimen M2). Both the FE simulation and the experimental test showed a neck type fracture.

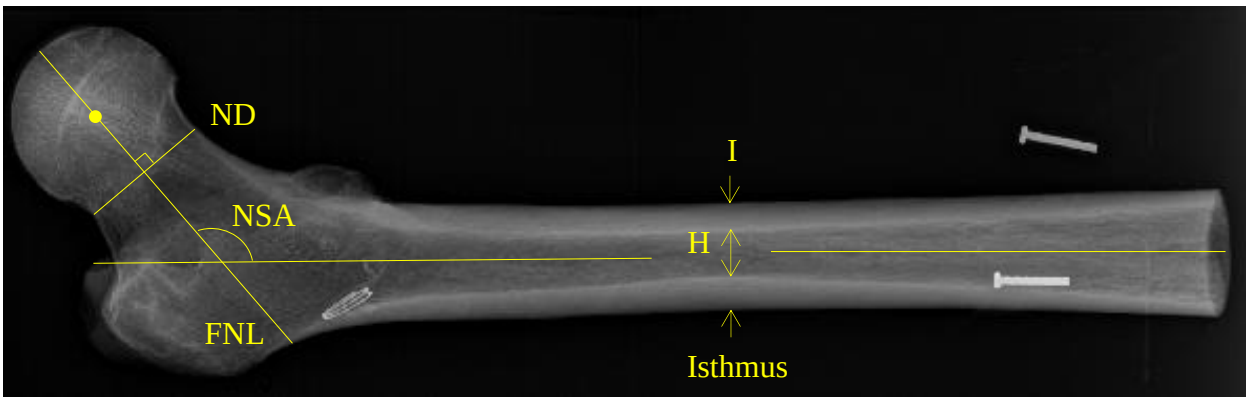

Figure 3 – Geometrical parameters of the femur. ND = width of femoral neck at its most narrow point, FNL = femoral neck length, NSA = neck shaft angle measured as angle between the femoral neck and the femoral shaft axes, and the cortical index (CI) at the femoral isthmus that equals to the ratio of the femoral diaphyseal diameter (I) minus the intramedullary canal diameter (H) over the femoral diaphyseal diameter; C = (I – H) / I

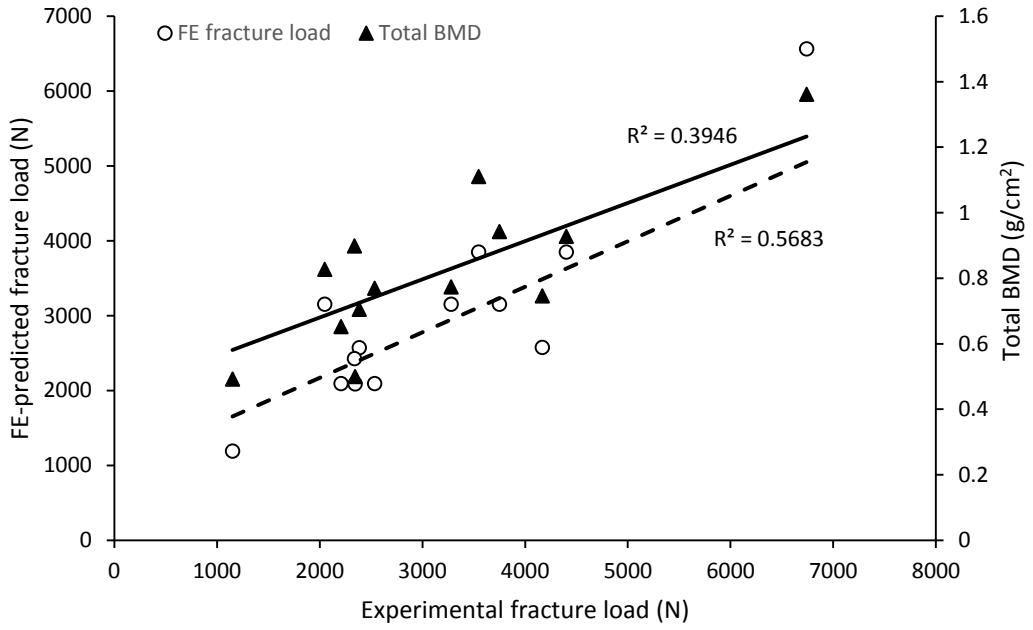

Figure 4 - The ability of FE to predict the actual (the experimental) fracture load compared to the ability of DXA-based BMD to predict the actual fracture load. Dashed line relates to FE fracture load data, solid line to BMD data.

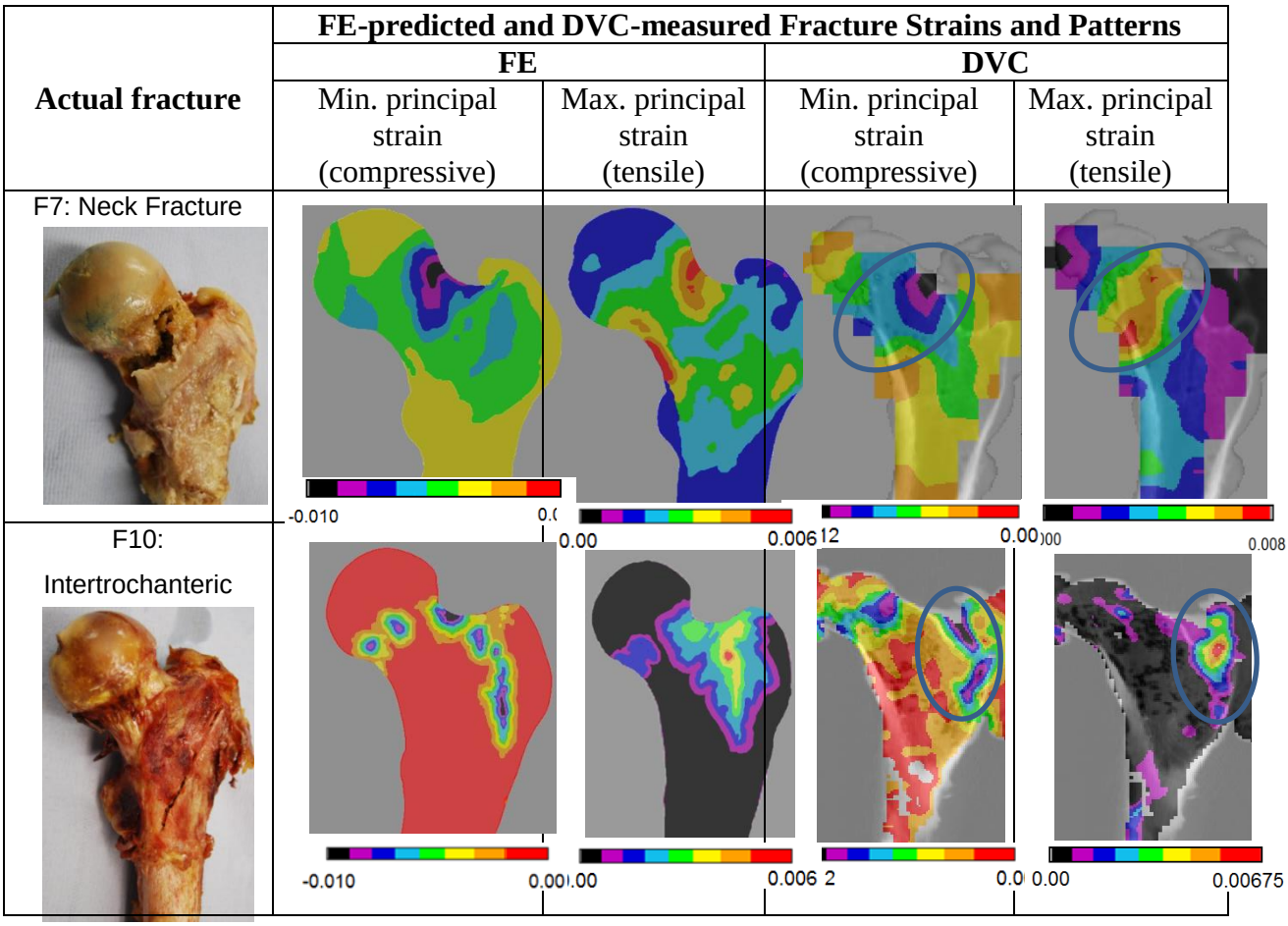

Figure 5 – Comparison of the experimentally observed fractures to the FE-predicted strain and fracture patterns as well as to the DVC-measured strains. Top row: Femur F7 exhibiting a femoral neck fracture. Bottom row: Femur F10 exhibiting an intertrochanteric fracture. High strain concentrations (circled) were apparent in regions where the femoral failure occurred and reflected the different fracture modes. Note, the DVC image of femur F10 is shown in an oblique view to better demonstrate the strain concentrations.

557 **Table 1** – Predicted and experimental fracture load and type listed in order of experimental fracture

558 load and according to gender.

Specimen	Total BMD (g/cm^2)	Fracture load (N)		Fracture type Observations in brackets.	
		Experiment	FE	Experiment	FE
F1	0.75	4166	2575	(Subcap oblique/basicervical) Neck	(Basicervical) Intertrochanteric
F2	0.94	3748	3154	(Subcapital) Neck	(Transcervical/basicervical) Neck
F3	0.77	3278	3153	(Basicervical/intertrochanteric) Intertrochanteric	(Basicervical/intertrochanteric) Intertrochanteric
F4	0.77	2534	2094	(Basicervical/intertrochanteric) Intertrochanteric	(Basicervical/transcervical) Intertrochanteric
F5	0.71	2382	2573	(Subcapital) Neck	(Transcervical) Neck
F6	0.50	2342	2091	(Basicervical/intertrochanter) Intertrochanteric	(Basicervical/intertrochanteric) Intertrochanteric
F7*	0.90	2339*	2425	(Transcervical) Neck	(Subcapital/basicervical) Neck
F8	0.65	2205	2091	(Basicervical) Intertrochanteric	(Cervical/basicervical) Neck
F9	0.83	2049	3153	(Basicervical) Intertrochanteric	(Trochanteric/basicervical) Intertrochanteric
F10*	0.49	1151*	1190	(Intertrochanteric/trochanteric) Intertrochanteric	(Intertrochanteric/trochanteric) Intertrochanteric
M1	1.36	6739	6565	(Intertrochanteric/basicervical) Intertertrochanteric	(Basicervical) Intertrochanteric
M2	0.93	4399	3850	(Subcapital/transcervical) Neck	(Cervical) Neck
M3	1.11	3547	3849	(Basicervical/intertrochanteric) Intertrochanteric	(Basicervical) Intertrochanteric
M4	1.00	-	3153	(Subcapital/transcervical) Neck	(Cervical + basicervical) Neck

559 *the recorded loads prior to failure (specimens used for DVC experiments)

560

561

562

563

564

Table 2 - Summary of the FE-predicted fractures and the observed fractures.

		Experimental	
		Neck	Intertrochanteric
FE	Neck	5	1
	Intertrochanteric	1	7

Table 3 – Comparison of specimen characteristics between fracture types.

				Females only		
	Neck fracture (n = 6)	**Intertrochanteric fracture (n = 7)**	**p-value**	**Neck fracture (n=4)**	**Intertrochanteric fracture (n=6)**	**p-value**
Female/male	4/2	6/1	0.56	4/0	6/0	*n/a*
Age (years)	73.8 ± 14.1	64.3 ± 13.6	0.24	76.8 ± 9.0	68.0 ± 10.4	0.21
Exp. Femoral strength (N)	3407 ± 984	2444 ± 797	0.09	3159 ± 938	2260 ± 692	0.12
Height (cm)	168.5 ± 8.4	163 ± 7.5	0.21	163.5 ± 3.1	160.2 ± 4.4	0.23
Weight (kg)	67.5 ± 24.2	74.6 ± 31.8	0.67	72.5 ± 29.6	72.0 ± 34.1	0.98
BMI	24.1 ± 9.6	27.9 ± 11.2	0.53	27.0 ± 10.9	27.7 ± 12.2	0.93
BMD at Neck (g/cm^2)	0.824 ± 0.092	0.669 ± 0.166	0.08	0.782 ± 0.092	0.624 ± 0.126	0.07
BMD at Wards (g/cm^2)	0.595 ± 0.064	0.503 ± 0.191	0.27	0.566 ± 0.040	0.445 ± 0.126	0.07
BMD Great Trochanter (g/cm^2)	0.729 ± 0.167	0.555 ± 0.185	0.11	0.649 ± 0.142	0.493 ± 0.090	0.07
Total BMD (g/cm^2)	0.870 ± 0.117	0.732 ± 0.213	0.19	0.823 ± 0.115	0.669 ± 0.146	0.12
Isthmus CI	0.59 ± 0.05	0.58 ± 0.07	0.83	0.57 ± 0.05	0.57 ± 0.08	0.90
Neck diameter (cm)	3.2 ± 0.3	3.2 ± 0.3	0.72	3.1 ± 0.2	3.1 ± 0.2	0.96
FNL (cm)	9.9 ± 0.7	9.9 ± 0.7	0.98	9.5 ± 0.3	9.7 ± 0.5	0.51
NSA (°)	127 ± 4.5	125 ± 5.6	0.72	124 ± 3.6	124 ± 3.4	0.80